

Constraining meV Axion Dark Matter with ALMA Observations of the Galactic Center Magnetar SGR 1745–2900

Javier De Miguel^{1,2,3,*}, Evanthia Hatziminaoglou^{4,1,2}, Frédéric Poidevin^{1,2},
Nanda Rea^{5,6}, Daniel L. Walker⁷, Davide De Grandis^{5,6}, and Jaime Prieto-Polo²

¹*Instituto de Astrofísica de Canarias, E-38200 La Laguna, Tenerife, Spain*

²*Departamento de Astrofísica, Universidad de La Laguna, E-38206 La Laguna, Tenerife, Spain*

³*The Institute of Physical and Chemical Research (RIKEN),*

Center for Advanced Photonics, 519-1399 Aramaki-Aoba, Aoba-ku, Sendai, Miyagi 980-0845, Japan

⁴*ESO, Karl-Schwarzschild-Str. 2, 85748 Garching bei München, Germany*

⁵*Institute of Space Sciences (ICE-CSIC), Campus UAB,*

C/ de Can Magrans s/n, Cerdanyola del Vallès (Barcelona) 08193, Spain

⁶*Institut d'Estudis Espacials de Catalunya (IEEC), 08034 Barcelona, Spain and*

⁷*UK ALMA Regional Centre Node, Jodrell Bank Centre for Astrophysics,
The University of Manchester, Manchester M13 9PL, UK*

(Dated: December 9, 2025)

We report a mm-wave search for axions from the magnetar SGR 1745–2900, based on 4.8 h of ALMA observations. No statistically significant features are detected between 133.99–135.78, 135.91–137.70, 145.99–147.78, and 147.99–149.78 GHz. Interpreting this null result via resonant conversion with a state-of-the-art star model and the dark-matter density expected at the Galactic Center, we constrain the axion–photon coupling at the level of $g_\gamma \gtrsim 2 \times 10^{-13} \text{ GeV}^{-1}$ within 0.55–0.62 meV, accessing for the first time the QCD axion parameter space near the meV scale.

INTRODUCTION

Axions are hypothetical pseudoscalar bosons arising from a compelling solution in quantum chromodynamics (QCD) to the strong-interaction charge–parity problem [1–3]. Owing to their very weak coupling to ordinary matter and small mass, axions are cosmologically well-motivated candidates for dark matter (DM) [4–6]—an invisible component inferred from astronomical observations decades ago but still undetected at the particle level [7–9]. The QCD axion and axion-like particles—similar to axions but with independent mass and coupling scales [10]—mix with photons in a static magnetic field via the Primakoff effect [11]. Classically, the axion–photon interaction relevant for this work reads

$$\mathcal{L} \supset g_\gamma \mathbf{E} \cdot \mathbf{B} a, \quad (1)$$

where g_γ is the axion–photon coupling factor, \mathbf{E} is the electromagnetic wave and \mathbf{B} the external static magnetic field, while a is the axion.

Magnetars are highly magnetized neutron stars (NSs)—compact stellar remnants that host the most powerful magnetic fields known in nature. When DM axions enter the NS magnetosphere, they can be resonantly converted into photons, producing an axion-induced emission feature superimposed on the intrinsic spectrum of the star [12–15]. For non-relativistic axions composing cold DM, this feature is expected to lie in the radio band of the electromagnetic spectrum [16–27].

The expected signal from ambient axions falling into the star and oscillating into photons scales with the DM

density at the source location and with the magnetic field strength at the conversion surface. As discussed in Ref. [28], the innermost region of the Galaxy departs significantly from a standard Navarro–Frenk–White (NFW) profile [29] and is expected to host axion densities several orders of magnitude larger than in the local halo [24, 25, 30]. In this context SGR 1745–2900 (RA, Dec 17:45:40.164, $-29:00:29.818$ [31]), with a surface magnetic field above 10^{14} G , emerges as one of the most favorable Galactic laboratories to probe axion DM. These advantages largely offset the observational challenges posed by its environment; the magnetar lies only $\sim 0.1 \text{ pc}$ from the brightest Galactic Center (GC) radio source Sagittarius A* (Sgr A*) and at a distance of about 8 kpc from Earth, which implies the d^{-2} geometric dilution of the signal. In this work we present the first dedicated search for axion DM using SGR 1745–2900 at millimeter wavelengths, aiming to identify narrow emission features arising from axion–photon conversion. The remainder of this Letter is organized as follows. We first describe the ob-

TABLE I. Per-SPW rms in the ON and nodding (ON–(OFF)) data after uv-plane modelling and subtraction of Sgr A*. All SPWs share the same correlator configuration and imaging parameters: $\Delta\nu_{\text{obs}} = 1788.9 \text{ MHz}$, $\delta\nu_{\text{ch}} = 7.811 \text{ MHz}$, synthesized beam FWHM $0.89 \times 0.73 \text{ arcsec}$ (PA = -88.1°), observations carried out between MJD 60683.0 and 60700.0, and total on-source integration time $t_{\text{int}} = 4.838 \text{ h}$.

SPW	Frequency [GHz]	rms [mJy/beam]	
		ON	ON–(OFF)
1	133.99–135.78	0.183	0.076
2	135.91–137.70	0.151	0.064
3	145.99–147.78	0.112	0.050
4	147.99–149.78	0.133	0.062

* jdemiguel@iac.es

servations, data reduction, and analysis procedure. We then employ state-of-the-art models to estimate the sensitivity to axion DM achieved with these data. Finally, we discuss the non-detection, its implications for axion models, and our overall conclusions.

OBSERVATIONS, DATA REDUCTION AND ANALYSIS

Observations were performed with the Atacama Large Millimeter/submillimeter Array (ALMA) in the 12-m setup with an angular resolution of 0.724 arcsec and a field of view of 41.039 arcsec centered on SGR 1745–2900, with a spectral resolution of 7.8113 MHz. A total of four spectral windows (SPWs) centered at 134.9, 136.8, 146.9, and 148.9 GHz, each with a bandwidth of ≈ 1.8 GHz in ALMA band 4 were observed for a total of 4.838 h effective integration time between 2025-01-08 and 2025-01-25.

Interferometric data were reduced as follows. All data reduction was performed with CASA (the Common Astronomy Software Applications, v6.6.1.17) [32] follow-

ing standard ALMA procedures. After initial flagging of corrupted visibilities, we applied flux, delay, band-pass, and gain calibrations provided by the observatory. Atmospheric transmission corrections were included through the water vapor radiometer data. We then carried out phase self-calibration using the bright continuum of Sgr A*, which improved coherence across all spectral windows [33]. The continuum emission was modeled and subtracted in the uv (Fourier) domain to minimize contamination, and spectral line image cubes were produced with pixel scales oversampling the synthesized beam. Residual narrow-band spectral features in the Sgr A* continuum, attributable to known molecular transitions—e.g., $^{13}\text{CH}_3\text{OH}$, $\text{H}(36)\alpha$, HC_3N , H_2CS , SO , ^{13}CS , CH_3NC , D_2CS , D^{13}CO , C_4H , DC_3N , CS , $\text{cis-CH}_2\text{OHCHO}$ —were cleaned during deconvolution. At the location of SGR 1745–2900, spectra were extracted by summing over the synthesized beam in each channel, and corrected for frequency-dependent beam size. The resulting spectra typically reach the theoretical noise level expected for the achieved integration time and channel width—see Table I. This reduction procedure ensures that the resulting cubes are optimised for isolating the spectrum of SGR 1745–2900 against the bright, variable Sgr A* background—see Fig. 1.

The reduced cube fits were analyzed as follows. From the calibrated data cubes we extracted spectra at the position of the magnetar SGR 1745–2900 (ON) using astrometry data [34] and at several nearby positions chosen to sample the local background (OFF). See Fig. 2 (top). The OFF spectra were averaged to form a reference $\langle \text{OFF} \rangle$, and the magnetar spectrum was differenced as $\text{DIFF} = \text{ON} - \langle \text{OFF} \rangle$. This subtraction removed large-scale GC emission and instrumental baselines while preserving narrow features at the source position. A high-pass filter was then applied to DIFF to suppress any residual continuum structure on $\gtrsim 1$ GHz scales—Fig. 2 (bottom). Within each SPW, a rolling median–absolute-deviation estimator was used to characterize the local noise per channel. These values were combined with a global rms to set adaptive clipping thresholds and construct per-channel weights, ensuring that regions affected by residual lines or artifacts contributed less to the analysis. Matched filtering was performed channel by channel using Gaussian kernels, with widths set by the expected axion-induced linewidth scaling with particle mass— $\Delta\nu/\nu \sim \Omega_* r_c \varepsilon^2/c$, with r_c being the conversion altitude, ε the eccentricity for an oblique rotator at which the intersection of a plane perpendicular to the rotation axis with the conversion surface is projected an ellipse, and c the speed of light [21, 35]. Each channel was fit with a weighted generalized least-squares regression that included a constant offset term, which accounts for any residual baseline level. For channels passing minimal coverage requirements— $>70\%$ unmasked—the fit returned an amplitude, its 1σ uncertainty, and the matched-filter signal-to-noise ratio (SNR). When the fitted amplitude was non-positive, a one-sided 95% confi-

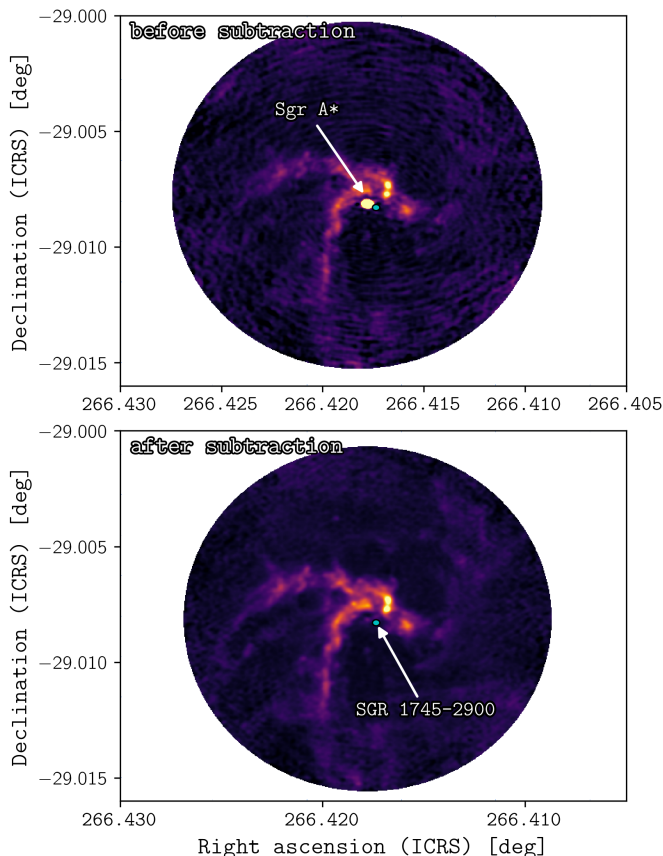


FIG. 1. ALMA 2-mm continuum of the GC before (top) and after (bottom) Sgr A* subtraction; the cyan ellipse marks the synthesized beam at the astrometry position of SGR 1745–2900.

TABLE II. Data analysis and matched-filter diagnostics by SPW; columns give the SPW index, fraction of channels masked (Masked frac.), fraction of channels accepted for analysis (Acceptance), median 1σ amplitude uncertainty in μJy (σ_A median), mean matched-filter signal-to-noise ratio ($\langle\text{SNR}\rangle$), standard deviation of the SNR distribution ($\sigma[\text{SNR}]$), and the number of positive excursions above 3σ and 3.5σ within the SPW ($N_{\geq 3\sigma}/N_{\geq 3.5\sigma}$). Bins with $\geq 3\sigma$ are 3.14σ at 134.016363 GHz and 3.41σ at 134.024175 GHz. These correspond to two consecutive bins ($\Delta\nu \approx 7.8$ MHz), much narrower than the expected axion line width (FWHM ~ 100 MHz, spanning several channels).

SPW	Masked frac. [%]	Acceptance [%]	σ_A median [μJy]	$\langle\text{SNR}\rangle$	$\sigma[\text{SNR}]$	$N_{\geq 3\sigma} / N_{\geq 3.5\sigma}$
1	19.6	77.8	45.36	0.030	1.208	2 / 0
2	14.8	82.6	39.99	0.039	0.982	0 / 0
3	23.9	73.5	35.35	0.038	0.816	0 / 0
4	12.6	84.8	36.32	-0.025	0.966	0 / 0

dence upper limit was reported. Quality-control diagnostics confirmed that $\sim 80\%$ of all channels were retained after masking and filtering, with 163 frequency bins masked and ruled out for science—135.149–135.493 GHz (45 bins), 136.480–136.738 GHz (36), 146.828–147.250 GHz (56), and 148.936–149.155 GHz (26)—, and that the matched-filter SNR distribution was centered at zero with unit variance (mean $\mu \approx 0.02$; standard deviation $\sigma \approx 1.01$), consistent with Gaussian noise—Fig. 3. Median 1σ flux uncertainties per SPW were in the range $(3.5\text{--}4.6) \times 10^{-5}$ Jy, corresponding to $\sim 40\text{--}50 \mu\text{Jy}/\text{beam}$ sensitivities when averaged over each SPW. See Table II. No significant positive excesses in the SNR above 3.5σ were found, while the final product is a frequency-dependent upper-limit spectrum that can be used to constrain narrow axion-induced features in the SGR 1745–2900 environment.

RESULTS

Goldreich & Julian (GJ) developed a NS model with a corotational, charge-separated plasma, with a balanced occupation of electron-proton pairs, fills the light-cylinder, assuming a perfect conductivity and homogeneity in the dipole field limit [36]. However, as shown by Beloborodov [37, 38], the GJ model cannot satisfactorily explain the mechanisms of a magnetar magnetosphere, sustained by the creation of pair cascades and particle migration through magnetic forces, accelerating the charges to relativistic velocities, giving rise to curvature radiation, synchrotron emission and inverse Compton scattering [39–41]. In the magnetospheric regions where axions may resonate and produce millimeter waves within a Beloborodov-like model of SGR 1745–2900, the resonance altitude is expected to be a significant fraction of the stellar radius. Under these conditions, pair multiplicities—defined as the number of electron-positron pairs produced per primary particle over the GJ density, $\mathcal{M} = n_e/n_{\text{GJ}}$ —of $\mathcal{M} \sim 100$ and a plasma Lorentz factor of $\gamma_p \sim 10$ are tenable. The charge density of the magnetospheric plasma is $n_e = (2\Omega_* B/e)(\mathcal{M}/\gamma_p)$, with $\Omega_* = 2\pi/P$ the angular velocity (P the rotation period) and e the elementary charge, leading to a plasma

frequency $\omega_p^2 = 4\pi\alpha n_e/m_e$, with α the fine structure constant and m_e the electron mass. Therefore, in order to interpret the results of the present manuscript, it is necessary to employ the mixing model capable of simultaneously account for a relativistic plasma and pair cascades in Ref. [42]. Following [37, 38], simulations with SGR 1745–2900 are here performed in the limit of a weakly twisted dipolar field for a misaligned rotator. Let \hat{m} be the magnetic axis, \hat{z} the rotation axis, and \hat{r} the photon propagation direction, θ_m the magnetic angle between the rotation and the magnetic axis with $f_1(t) = |3\cos\theta\hat{m}\cdot\hat{r} - \cos\theta_m|$ encoding time dependence. Resonant conversion occurs when $m_a \simeq \omega_p$, at a radius

$$r_c = 224 \text{ km } f_1^{1/3}(t) \frac{R_*}{10 \text{ km}} \left[\frac{B_0}{10^{14} \text{ G}} \frac{1 \text{ s}}{P} \left(\frac{1 \text{ GHz}}{m_a} \right)^2 \frac{\mathcal{M}}{\gamma_p} \right]^{1/3}, \quad (2)$$

with R_* the stellar radius. The axion velocity at the conversion point is $v_a^2 \simeq 2GM_*/r_c$, with G the gravitational constant and M_* the stellar mass. The axion-induced line is broadened by various mechanisms [17, 21, 35, 43]; here the plasma-mirror scenario is adopted. The resulting flux density is [42]

$$S_\nu = 1.6 \times 10^{-5} \mu\text{Jy } f_2(t) \left(\frac{1 \text{ kpc}}{d} \right)^2 \left(\frac{g_\gamma}{10^{-12} \text{ GeV}^{-1}} \right)^2 \times \frac{R_*}{10 \text{ km}} \left(\frac{m_a}{1 \text{ GHz}} \right)^{4/3} \left(\frac{B_0}{10^{14} \text{ G}} \right)^{1/3} \left(\frac{\Omega_*}{1 \text{ Hz}} \right)^{-8/3} \times \frac{\rho_a}{0.4 \text{ GeV cm}^{-3}} \frac{M_*}{1 M_\odot} \frac{200 \text{ km s}^{-1}}{v_0} \frac{v_a}{c} \left(\frac{\mathcal{M}}{\gamma_p} \right)^{-3/2}, \quad (3)$$

with $f_2(t) = [3(\hat{m}\cdot\hat{r})^2 + 1] f_1^{-4/3}(t)$, v_0 the radial velocity, ρ_a the axion density. The telescope sensitivity in terms

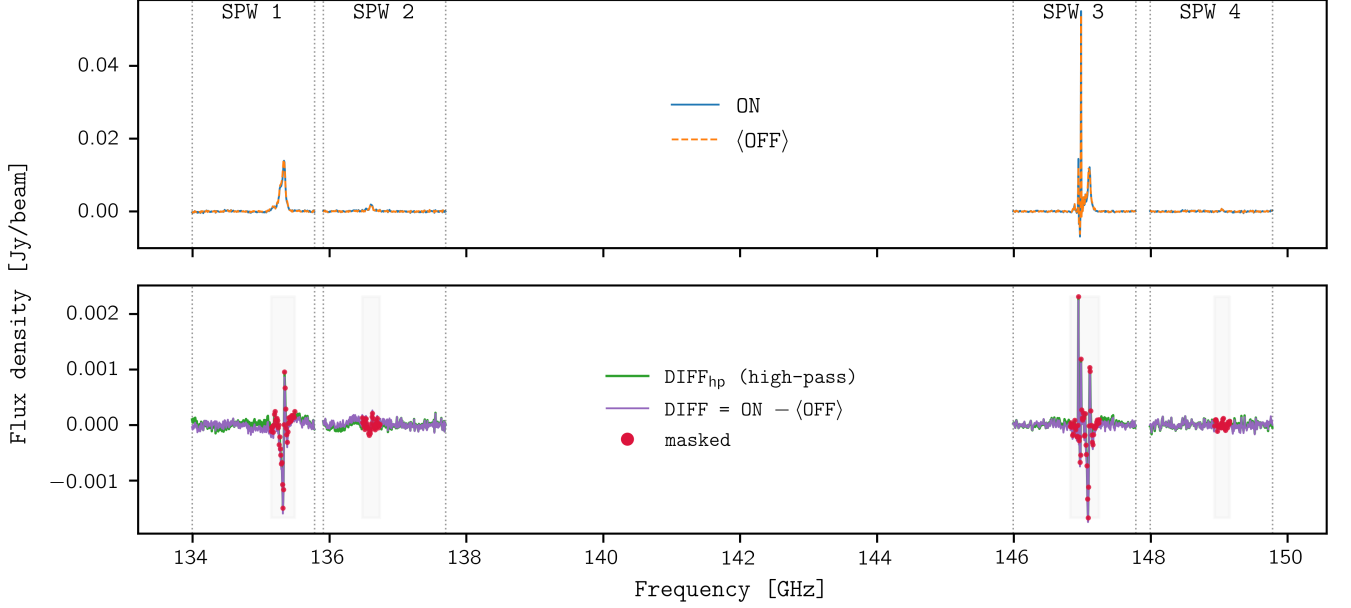


FIG. 2. Top: raw ON–source spectrum toward SGR 1745–2900 (blue) and averaged OFF reference (orange), shown per spectral window (SPW; vertical dotted lines). Bottom: differenced spectrum, ON–⟨OFF⟩ (purple), and its high–pass (hp) filtered version (green). Masked channels are marked in red with shaded regions indicating their extent.

of coupling strength follows as

$$g_\gamma \gtrsim 2.5 \times 10^{-10} \text{ GeV}^{-1} \left(\frac{S_\nu}{1 \mu\text{Jy}} \right)^{1/2} f_2^{-1/2}(t) \frac{d}{1 \text{ kpc}} \times \left(\frac{10 \text{ km}}{R_*} \right)^{1/2} \left(\frac{1 \text{ GHz}}{m_a} \right)^{2/3} \left(\frac{10^{14} \text{ G}}{B_0} \right)^{1/6} \times \left(\frac{\Omega_*}{1 \text{ Hz}} \right)^{4/3} \left(\frac{0.4 \text{ GeV cm}^{-3}}{\rho_a} \right)^{1/2} \left(\frac{1 M_\odot}{M_*} \right)^{1/2} \times \left(\frac{v_0}{200 \text{ km s}^{-1}} \right)^{1/2} \left(\frac{c}{v_a} \right)^{1/2} \left(\frac{\mathcal{M}}{\gamma_p} \right)^{3/4}. \quad (4)$$

From the upper-limit amplitudes derived in the

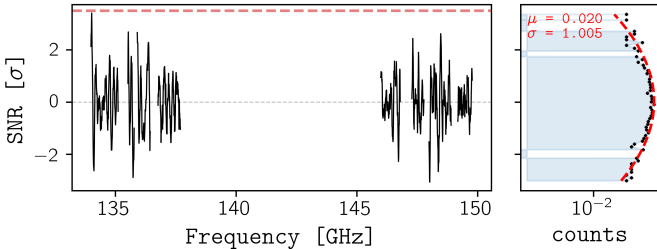


FIG. 3. Left: distribution of SNR across frequency after applying the matched-filter pipeline. Horizontal dashed lines indicate the zero level and the 3.5σ detection threshold (red). Right: histogram of SNR values for all accepted channels (black), compared to a rescaled Gaussian with mean μ and standard deviation σ (red dashed).

matched-filter analysis, we computed the corresponding constraints on the axion–photon coupling strength, g_γ , using Eq. 4. Each spectral channel was mapped to an axion mass through the resonance condition, with the conversion radius, plasma multiplicity, and Lorentz factor obtained from magnetospheric profiles adapted to Beloborodov-type models. The axion velocity at the resonance region was included via gravitational acceleration, while geometric and temporal factors were treated explicitly. In particular, the time-dependent factor $f_2(t)$ was averaged over one stellar rotation to account for the multi-hour integration of our ALMA observations. For every contiguous frequency run, we computed the one-sided 95% confidence level upper limits g_γ^{95} , which are summarized in Table III. In Fig. 4, we adopt the NFW profile modified to include a spike (sp) with radial index $\gamma_{\text{sp}} = 7/3$ and radius $R_{\text{sp}} = 0.1 \text{ kpc}$, consistent with the 99.7% upper limit on deviations from a purely black-hole orbit of the S2 star around Sgr A*, following Refs. [24, 25, 28, 30]. This model yields a DM density of $\rho_{\text{DM}} \sim 6.4 \times 10^8 \text{ GeV cm}^{-3}$ at the position of the magnetar. The stellar parameters adopted in our three benchmark models (*light*, *canonical*, *heavy*) are derived self-consistently from the mass–radius–moment-of-inertia relations implied by the BSk24 nuclear equation of state (EoS) [54]. For each assumed gravitational mass M_* , BSk24 yields a unique radius $R(M_*)$ and moment of inertia $I(M_*)$. The corresponding moment of inertia then determines the dipolar magnetic field through the usual spin-down expression $B_0 \simeq 6.4 \times 10^{19} I_{45}^{1/2} (P\dot{P})^{1/2} \text{ G}$, where $I_{45} \equiv I/10^{45} \text{ g cm}^2$, P is measured in seconds and

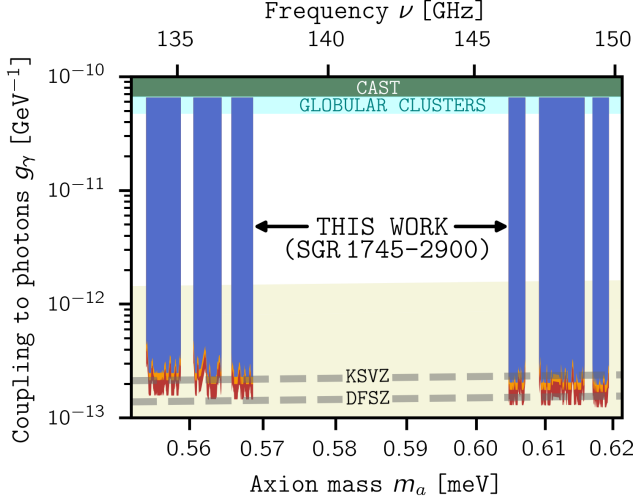


FIG. 4. 95% CL constraints on g_γ from ALMA observations of SGR 1745–2900, shown for three NS configurations. The blue shaded area corresponds to a *light* star (M_*, R_*, B_0) = $(1.17 M_\odot, 12.54 \text{ km}, 8.4 \times 10^{14} \text{ G})$; the red area to the *canonical* NS ($1.40 M_\odot, 12.59 \text{ km}, 9.52 \times 10^{14} \text{ G}$); and the red filled region to a *heavy* model ($2.10 M_\odot, 12.53 \text{ km}, 1.14 \times 10^{15} \text{ G}$). For all three configurations we assume $P = 3.76 \text{ s}$ [31], $v_0 = 236 \text{ km s}^{-1}$ [44], $\theta \simeq 20^\circ$, $\theta_m \simeq 10^\circ$, $\varepsilon \approx 0.9$ and a Beloborodov magnetosphere with $\mathcal{M} \simeq 50$ and $\gamma_p \simeq 2$ [37, 38]. The ambient axion density is $6 \times 10^8 \text{ GeV cm}^{-3}$ [28, 30]. Results are compared with CAST limits [45, 46] and globular-cluster bounds [47, 48]. The *phenomenologically preferred* axion window is shown in beige [49], together with benchmark QCD-axion models (KSVZ, DFSZ) [50–53].

\dot{P} in ss^{-1} . The observed NS population spans masses from about $1.2 M_\odot$ [55] to $2.1 M_\odot$ [56], and within this physical range BSk24 yields $M_* = 1.17 M_\odot \rightarrow R = 12.54 \text{ km}$, $I_{45} = 1.55$, $B_0 = 8.4 \times 10^{14} \text{ G}$, and $M_* = 2.1 M_\odot \rightarrow R = 12.13 \text{ km}$, $I_{45} = 2.78$, $B_0 = 1.14 \times 10^{15} \text{ G}$. The role of 3D magnetospheric structure, and its relation to the simplified 1D framework adopted here, is discussed in the Supplemental Material.

TABLE III. One-sided 95% CL constraints on g_γ per SPW for the *canonical* NS model (see Fig. 4). For each SPW we report the minimum, mean, and median channel-wise g_γ^{95} values, assuming an axion density $\rho_{\text{sp}} = 6.4 \times 10^8 \text{ GeV cm}^{-3}$ [28, 30].

SPW	$g_\gamma^{95} [10^{-13} \text{ GeV}^{-1}]$		
	minimum	mean	median
1	2.13	2.48	2.27
2	1.98	2.27	2.16
3	1.75	1.98	1.81
4	1.69	1.95	1.83

CONCLUSIONS

SGR 1745–2900 is one of the most promising astrophysical targets to probe axion DM, given its intense surface magnetic field and the expected density spike in the vicinity of Sgr A*, the GC. Since the resonance condition for axion–photon conversion depends on the ratio \mathcal{M}/γ_p —with \mathcal{M} the pair multiplicity factor and γ_p the plasma Lorentz factor—values $\mathcal{M}/\gamma_p \sim 1$ enable efficient conversion in the magnetosphere at microwave frequencies, while $\mathcal{M}/\gamma_p \gg 1$ extends the accessible band from microwaves into the millimeter regime. The present study focuses on the latter case. We have carried out the first mm-wave search for axion DM using 4.8 h of ALMA observations of SGR 1745–2900, finding no statistically significant evidence for axion-induced emission lines. Under a Beloborodov magnetospheric model with axion–photon resonant conversion, the null result can be translated into exclusion limits in the sub- to near-meV mass range—0.554–0.562, 0.562–0.570, 0.604–0.611, and 0.612–0.620 meV—, probing the QCD axion at high-frequency, shown in Fig. 4. This approach provides access to a region of parameter space that has remained inaccessible to other methods. Our search is therefore complementary to next-generation laboratory experiments [57–61], and can be extended in both sensitivity and frequency coverage by the same methodology and by parallel experimental strategies.

ACKNOWLEDGEMENTS

This paper makes use of the following ALMA data: ADS/JAO.ALMA#2024.1.00310. The project that gave rise to these results received the support of a fellowship from “la Caixa” Foundation (ID 100010434). The fellowship code is LCF/BQ/PI24/12040023”. J.D.M. acknowledges support from the Spanish Ministry of Science, Innovation and Universities and the Agency (EUR2024-153552 financed by MICIU/AEI/10.13039/501100011033). F.P. acknowledges support from the MICINN under grant numbers PID2022-141915NB-C21. N.R. is supported by the ERC via the Consolidator grant “MAGNESIA” (No. 817661), the ERC Proof of Concept “DeepSpacePULSE” (No. 101189496), the Spanish grant PID2023-153099NA-I00, and by the program Unidad de Excelencia María de Maeztu CEX2020-001058-M. D.D.G. is supported by a Juan de la Cierva fellowship (JDC2023-052264-I). Thanks L. Maud, H. Messias, and A. Richards for support.

-
- [1] R. D. Peccei and H. R. Quinn, CP conservation in the presence of pseudoparticles, *Phys. Rev. Lett.* **38**, 1440 (1977).
- [2] S. Weinberg, A new light boson?, *Phys. Rev. Lett.* **40**, 223 (1978).
- [3] F. Wilczek, Problem of strong p and t invariance in the presence of instantons, *Phys. Rev. Lett.* **40**, 279 (1978).
- [4] L. Abbott and P. Sikivie, A cosmological bound on the invisible axion, *Physics Letters B* **120**, 133 (1983).
- [5] M. Dine and W. Fischler, The not-so-harmless axion, *Physics Letters B* **120**, 137 (1983).
- [6] J. Preskill, M. B. Wise, and F. Wilczek, Cosmology of the invisible axion, *Physics Letters B* **120**, 127 (1983).
- [7] F. Zwicky, Die Rotverschiebung von extragalaktischen Nebeln, *Helvetica Physica Acta* **6**, 110 (1933).
- [8] V. C. Rubin and J. Ford, W. Kent, Rotation of the Andromeda Nebula from a Spectroscopic Survey of Emission Regions, *Astrophys. J.* **159**, 379 (1970).
- [9] G. Bertone and D. Hooper, History of dark matter, *Reviews of Modern Physics* **90**, 045002 (2018), arXiv:1605.04909 [astro-ph.CO].
- [10] E. Massó and R. Toldrà, Light spinless particle coupled to photons, *Phys. Rev. D* **52**, 1755 (1995).
- [11] H. Primakoff, Photoproduction of neutral mesons in nuclear electric fields and the mean life of the neutral meson, *Phys. Rev.* **81**, 899 (1951).
- [12] N. Iwamoto, Axion Emission from Neutron Stars, *Phys. Rev. Lett.* **53**, 1198 (1984).
- [13] G. Raffelt and L. Stodolsky, Mixing of the photon with low-mass particles, *Phys. Rev. D* **37**, 1237 (1988).
- [14] D. E. Morris, Axion Mass Limits From Pulsar X-rays, *Phys. Rev. D* **34**, 843 (1986).
- [15] M. Yoshimura, Resonant axion-photon conversion in magnetized plasma, *Phys. Rev. D* **37**, 2039 (1988).
- [16] D. Lai and J. Heyl, Probing Axions with Radiation from Magnetic Stars, *Phys. Rev. D* **74**, 123003 (2006), arXiv:astro-ph/0609775.
- [17] A. Hook, Y. Kahn, B. R. Safdi, and Z. Sun, Radio signals from axion dark matter conversion in neutron star magnetospheres, *Phys. Rev. Lett.* **121**, 241102 (2018).
- [18] F. P. Huang, K. Kadota, T. Sekiguchi, and H. Tashiro, Radio telescope search for the resonant conversion of cold dark matter axions from the magnetized astrophysical sources, *Phys. Rev. D* **97**, 123001 (2018), arXiv:1803.08230 [hep-ph].
- [19] M. Leroy, M. Chianese, T. D. P. Edwards, and C. Weniger, Radio Signal of Axion-Photon Conversion in Neutron Stars: A Ray Tracing Analysis, *Phys. Rev. D* **101**, 123003 (2020), arXiv:1912.08815 [hep-ph].
- [20] B. R. Safdi, Z. Sun, and A. Y. Chen, Detecting Axion Dark Matter with Radio Lines from Neutron Star Populations, *Phys. Rev. D* **99**, 123021 (2019), arXiv:1811.01020 [astro-ph.CO].
- [21] R. A. Battye, B. Garbrecht, J. I. McDonald, F. Pace, and S. Srinivasan, Dark matter axion detection in the radio/mm waveband, *Phys. Rev. D* **102**, 023504 (2020).
- [22] S. J. Witte, D. Noordhuis, T. D. P. Edwards, and C. Weniger, Axion-photon conversion in neutron star magnetospheres: The role of the plasma in the Goldreich-Julian model, *Phys. Rev. D* **104**, 103030 (2021), arXiv:2104.07670 [hep-ph].
- [23] R. A. Battye, B. Garbrecht, J. I. McDonald, and S. Srinivasan, Radio line properties of axion dark matter conversion in neutron stars, *JHEP* **09**, 105, arXiv:2104.08290 [hep-ph].
- [24] J. Darling, Search for Axionic Dark Matter Using the Magnetar PSR J1745-2900, *Phys. Rev. Lett.* **125**, 121103 (2020), arXiv:2008.01877 [astro-ph.CO].
- [25] J. Darling, New Limits on Axionic Dark Matter from the Magnetar PSR J1745-2900, *Astrophys. J. Lett.* **900**, L28 (2020), arXiv:2008.11188 [astro-ph.CO].
- [26] J. De Miguel and C. Otani, Superdense beaming of axion dark matter in the vicinity of the light cylinder of pulsars, *JCAP* **08** (08), 026, arXiv:2111.01746 [astro-ph.HE].
- [27] J. De Miguel and C. Otani, Axion-photon multimessenger astronomy with giant flares, *Phys. Rev. D* **106**, L041302 (2022).
- [28] P. J. McMillan, The mass distribution and gravitational potential of the milky way, *Monthly Notices of the Royal Astronomical Society* **465**, 76 (2016).
- [29] J. F. Navarro, C. S. Frenk, and S. D. M. White, The Structure of cold dark matter halos, *Astrophys. J.* **462**, 563 (1996), arXiv:astro-ph/9508025.
- [30] T. Lacroix, Dynamical constraints on a dark matter spike at the Galactic centre from stellar orbits, *Astronomy & Astrophysics* **619**, A46 (2018), arXiv:1801.01308 [astro-ph.GA].
- [31] K. Mori *et al.*, NuSTAR discovery of a 3.76-second transient magnetar near Sagittarius A*, *Astrophys. J. Lett.* **770**, L23 (2013), arXiv:1305.1945 [astro-ph.HE].
- [32] B. Bean *et al.* (CASA Team), CASA, Common Astronomy Software Applications for Radio Astronomy, *Publ. Astron. Soc. Pac.* **134**, 114501 (2022), arXiv:2210.02276 [astro-ph.IM].
- [33] E. Albentosa-Ruiz, I. Martí-Vidal, C. Goddi, and A. Mus, A novel calibration and imaging method for alma observations of sgr a* (2025), arXiv:2503.11258 [astro-ph.IM].
- [34] F. Yusef-Zadeh, R. Schödel, M. Wardle, H. Bushouse, W. Cotton, M. J. Royster, D. Kunneriath, D. A. Roberts, and E. Gallego-Cano, Alma and vla observations of emission from the environment of sgr a*, *Monthly Notices of the Royal Astronomical Society* **470**, 4209 (2017), <https://academic.oup.com/mnras/article-pdf/470/4/4209/18800855/stx1439.pdf>.
- [35] J. W. Foster, Y. Kahn, O. Macias, Z. Sun, R. P. Eatough, V. I. Kondratiev, W. M. Peters, C. Weniger, and B. R. Safdi, Green bank and effelsberg radio telescope searches for axion dark matter conversion in neutron star magnetospheres, *Phys. Rev. Lett.* **125**, 171301 (2020).
- [36] P. Goldreich and W. H. Julian, Pulsar Electrodynamics, *Astrophys. J.* **157**, 869 (1969).
- [37] A. M. Beloborodov, ON THE MECHANISM OF HARD x-RAY EMISSION FROM MAGNETARS, *The Astrophysical Journal* **762**, 13 (2012).
- [38] A. M. Beloborodov, ELECTRON-POSITRON FLOWS AROUND MAGNETARS, *The Astrophysical Journal* **777**, 114 (2013).
- [39] M. A. Ruderman and P. G. Sutherland, Theory of pulsars: polar gaps, sparks, and coherent microwave radiation., *Astrophys. J.* **196**, 51 (1975).

- [40] J. Arons and E. T. Scharlemann, Pair formation above pulsar polar caps: structure of the low altitude acceleration zone., *Astrophysical Journal* **231**, 854 (1979).
- [41] M. Kramer, K. M. Xilouris, A. Jessner, D. R. Lorimer, R. Wielebinski, and A. G. Lyne, Origin of pulsar radio emission. I. High frequency data., *Astronomy and Astrophysics* **322**, 846 (1997).
- [42] J. De Miguel, Retuning radio astronomy for axion dark matter with neutron stars, *Physics Letters B* **862**, 139328 (2025).
- [43] F. P. Huang, K. Kadota, T. Sekiguchi, and H. Tashiro, Radio telescope search for the resonant conversion of cold dark matter axions from the magnetized astrophysical sources, *Phys. Rev. D* **97**, 123001 (2018).
- [44] G. C. Bower *et al.*, The Proper Motion of the Galactic Center Pulsar Relative to Sagittarius A*, *Astrophys. J.* **798**, 120 (2015), arXiv:1411.0399 [astro-ph.HE].
- [45] K. Altenmüller, V. Anastassopoulos, S. Argüedas-Cuendis, S. Aune, J. Baier, K. Barth, H. Bräuninger, G. Cantatore, F. Caspers, J. F. Castel, S. A. Çetin, F. Christensen, C. Cogollos, T. Dafni, M. Davenport, T. A. Decker, K. Desch, D. Díez-Ibáñez, B. Döbrich, E. Ferrer-Ribas, H. Fischer, W. Funk, J. Galán, J. A. García, A. Gardikiotis, I. Giomataris, J. Golm, C. H. Hailey, M. D. Hasinoff, D. H. H. Hoffmann, I. G. Irastorza, J. Jacoby, A. C. Jakobsen, K. Jakovčić, J. Kaminski, M. Karuza, S. Kostoglou, C. Krieger, B. Lakić, J. M. Laurent, G. Luzón, C. Malbrunot, C. Margalejo, M. Maroudas, L. Miceli, H. Mirallas, P. Navarro, L. Obis, A. Özbey, K. Özbozduman, T. Papaevangelou, O. Pérez, M. J. Pivovarov, M. Rosu, E. Ruiz-Chóliz, J. Ruz, S. Schmidt, M. Schumann, Y. K. Semertzidis, S. K. Solanki, L. Stewart, T. Vafeiadis, J. K. Vogel, and K. Zioutas (CAST Collaboration), New upper limit on the axion-photon coupling with an extended cast run with a xe-based micromegas detector, *Phys. Rev. Lett.* **133**, 221005 (2024).
- [46] V. Anastassopoulos *et al.* (CAST), New CAST Limit on the Axion-Photon Interaction, *Nature Phys.* **13**, 584 (2017), arXiv:1705.02290 [hep-ex].
- [47] A. Ayala, I. Domínguez, M. Giannotti, A. Mirizzi, and O. Straniero, Revisiting the bound on axion-photon coupling from Globular Clusters, *Phys. Rev. Lett.* **113**, 191302 (2014), arXiv:1406.6053 [astro-ph.SR].
- [48] M. J. Dolan, F. J. Hiskens, and R. R. Volkas, Advancing globular cluster constraints on the axion-photon coupling, *Journal of Cosmology and Astroparticle Physics* **2022** (10), 096, arXiv:2207.03102 [hep-ph].
- [49] L. Di Luzio, F. Mescia, and E. Nardi, Redefining the Axion Window, *Phys. Rev. Lett.* **118**, 031801 (2017), arXiv:1610.07593 [hep-ph].
- [50] J. E. Kim, Weak-interaction singlet and strong CP invariance, *Phys. Rev. Lett.* **43**, 103 (1979).
- [51] M. A. Shifman, A. Vainshtein, and V. I. Zakharov, Can confinement ensure natural cp invariance of strong interactions, *Nuclear Physics* **166**, 493 (1980).
- [52] M. Dine, W. Fischler, and M. Srednicki, A simple solution to the strong cp problem with a harmless axion, *Physics Letters B* **104**, 199 (1981).
- [53] A. P. Zhitnitskii, Possible suppression of axion-hadron interactions, *Sov. J. Nucl. Phys. (Engl. Transl.)*; (United States) **31:2**, (1980).
- [54] Y. D. Mutafchieva, Z. K. Stoyanov, N. Chamel, J. M. Pearson, and L. M. Mihailov, Unified equation of state for the outer and inner crusts of magnetars, *Journal of Physics: Conference Series* **1555**, 012015 (2020).
- [55] J. G. Martinez, K. Stovall, P. C. C. Freire, J. S. Deneva, F. A. Jenet, M. A. McLaughlin, M. Bagchi, S. D. Bates, and A. Ridolfi, Pulsar j0453+1559: A double neutron star system with a large mass asymmetry, *The Astrophysical Journal* **812**, 143 (2015).
- [56] H. T. Cromartie, E. Fonseca, S. M. Ransom, P. B. Demorest, Z. Arzoumanian, H. Blumer, P. R. Brook, M. E. DeCesar, T. Dolch, J. A. Ellis, R. D. Ferdman, E. C. Ferrara, N. Garver-Daniels, P. A. Gentile, M. L. Jones, M. T. Lam, D. R. Lorimer, R. S. Lynch, M. A. McLaughlin, C. Ng, D. J. Nice, T. T. Pennucci, R. Spiewak, I. H. Stairs, K. Stovall, J. K. Swiggum, and W. W. Zhu, Relativistic Shapiro delay measurements of an extremely massive millisecond pulsar, *Nature Astronomy* **4**, 72 (2020), arXiv:1904.06759 [astro-ph.HE].
- [57] J. De Miguel, A dark matter telescope probing the 6 to 60 GHz band, *JCAP* **04**, 075, arXiv:2003.06874 [physics.ins-det].
- [58] J. De Miguel, J. F. Hernández-Cabrera, E. Hernández-Suárez, E. Joven-Álvarez, C. Otani, and J. Alberto Rubiño Martín (On behalf of the DALI Collaboration), Discovery prospects with the dark-photons & axion-like particles interferometer, *Phys. Rev. D* **109**, 062002 (2024).
- [59] J. F. Hernández-Cabrera, J. De Miguel, E. Joven Álvarez, E. Hernández-Suárez, J. A. Rubiño-Martín, and C. Otani, A forecast of the sensitivity of the dali experiment to galactic axion dark matter, *Symmetry* **16**, 10.3390/sym16020163 (2024).
- [60] J. F. Hernández-Cabrera, J. De Miguel, E. Hernández-Suárez, E. Joven-Álvarez, H. Lorenzo-Hernández, C. Otani, M. A. Rapado-Tamarit, and J. A. Rubiño-Martín (DALI), Experimental measurement of the quality factor of a Fabry-Pérot open-cavity axion haloscope, *JINST* **19** (01), P01022, arXiv:2310.16013 [hep-ph].
- [61] J. De Miguel, A. Kryemadhi, and K. Zioutas (On behalf of the DALI Collaboration), Dali sensitivity to streaming axion dark matter, *Phys. Rev. D* **111**, 023016 (2025)